cordings. Single-channel recordings were done in the excised inside-out membrane patch configuration, as described (7) [Y. Tsuura *et al., Diabetes* **42**, 861 (1992)]. The intracellular solution contained 110 mM potassium aspartate, 30 mM KCl, 2 mM $MgSO_4$, 1 mM EGTA, 0.084 mM $CaCl_2$, and 10 mM MOPS (pH 7.2). Dipotassium ATP (1 μM) was always added to the intracellular solution. The pipette solution contained 140 mM KCl, 2 mM $CaCl_2$, and 5 mM MOPS (pH 7.4). Recordings were made at 20° to 22°C.

23. COSm6 cells were plated at a density of 2.5×10^5 cells per well (30-mm six-well dish) and cultured in DMEM (high glucose) (DMEM-HG) supplemented with fetal calf serum (10 percent). The following day, pCMVmBIR (5 μg) and haSUR cDNA (5 μg), cloned into the pECE expression vector (5), were cotransfected into COSm6 cells with DEAE-dextran (5 mg/ml). Cells were incubated for 2 min in Hepes-buffered salt solution containing dimethyl sulfoxide (10 percent) and for 4 hours in DMEM-HG containing fetal bovine serum (FBS) (2 percent) and chloroquine (10 μM) and then returned to DMEM-HG containing FBS (10 percent). After 24 hours, ^{86}RbCl (1 μCi/ml) was added in fresh DMEM-HG containing FBS (10 percent). Cells were incubated for 12 to 24 hours before efflux was measured as described (*18*). Briefly, cells were incubated for 30 min at 25°C in Krebs-Ringer solution containing ^{86}RbCl (1 μCi/ml) with or without oligomycin (2.5 μg/ml) and 1 mM 2-deoxy-D-glucose. Cells were washed once in Rb-free Krebs-Ringer solution, with or without added metabolic inhibitors and glibenclamide. Time points were taken by removing all the medium from the cells and replacing it with fresh medium. Portions of the medium from each time point were counted, and the values were summed to determine flux. The data are presented as the percentage of total cellular $^{86}Rb^+$ released. Dose-response curves were obtained with sulfonylureas with metabolic inhibitors or diazoxide without metabolic inhibitors. The percent response was estimated from the efflux values at 40 min; the end points were used as 0 and 100 percent response, respectively. All of the curves are the averages of two or more independent experiments; the error bars are standard deviations. Efficiencies of transfection, estimated from β-galactosidase staining and by recording ATP-sensitive potassium channel activity from excised inside-out patches from randomly chosen cells, were >75 percent and 34 out of 35, respectively. These high levels of transfection gave patches with large numbers of K_{ATP} channels and were unsuitable for recording single channels.
24. N. C. Sturgess, R. Z. Kozlowski, C. A. Carrington, C. N. Hales, M. L. J. Ashford, *Br. J. Pharmacol.* **95**, 83 (1988).
25. G. Trube, P. Rorsman, T. Ohno-Shsaku, *Pfluegers Arch.* **407**, 493 (1986).
26. The plasmid pGEM3Z (Promega) containing a full-length cDNA encoding mBIR and pBluescript SK(+) containing a full-length cDNA encoding haSUR were linearized with Hind III and with Spe I, respectively, and transcribed in vitro, according to the manufacturer's instructions. *Xenopus* oocytes were treated with collagenase, and defolliculated oocytes were selected under microscopy [F. Wibrand *et al., Proc. Natl. Acad. Sci. U.S.A.* **89**, 5133 (1992)]. *Xenopus* oocytes were injected with 60 nl of H_2O alone, mBIR cRNA alone (20 ng), haSUR cRNA alone (40 ng), or mBIR cRNA (20 ng) and haSUR cRNA (40 ng). After 2 to 3 days, electrophysiological measurements were made with the two-electrode voltage clamp technique, as described (7). The microelectrodes were filled with 3 M KCl; the resistance was 0.3 to 1.0 megohm. The extracellular bathing solution contained 90 mM KCl, 3 mM $MgCl_2$, and 5 mM Hepes (pH 7.4). Recordings were made at 20° to 22°C.
27. N. Namba *et al.*, unpublished data.
28. N. Namba *et al.*, unpublished results.
29. D. L. Cook and C. N. Hales, *Nature* **311**, 271 (1984); I. Findlay, M. J. Dunne, O. H. Petersen, *J. Membr. Biol.* **88**, 165 (1985); P. Rorsman and G. Trube, *Pfluegers Arch.* **405**, 305 (1985); S. Misler, L. C. Falke, K. Gillis, M. L. McDaniel, *Proc. Natl. Acad. Sci. U.S.A.* **83**, 7119 (1986).
30. Y. Yamada *et al., Proc. Natl. Acad. Sci. U.S.A.* **89**, 251 (1992).
31. The nucleotide sequences have been deposited in the Genome Sequence Data Base, the DNA Data Bank of Japan, the European Molecular Biology Laboratory, and the National Center for Biotechnology Information nucleotide sequence databases with the accession numbers D50581 and D50582 for the mBIR cDNA and the hBIR gene, respectively.
32. We thank Y. Tsuura and Y. Kubo for contributing to an initial part of the electrophysiological studies, D. Cook for helpful discussion, and K. Sakurai, A. Tamamoto, H. Aida, R. Lee, and M. Lopez for technical assistance. Supported by Scientific Research Grants from the Ministry of Education, Science and Culture and from the Ministry of Health and Welfare, Japan; by grants from Ohtsuka Pharmaceutical Ltd., Novo Nordisk Pharma Ltd., Yamanouchi Foundation for Research on Metabolic Disorders, and NIH (grant DK44311) (J.B.); and by the Houston Endowment (L.A.-B.).

21 August 1995; accepted 19 October 1995

Crystal Structure of the Xanthine Oxidase–Related Aldehyde Oxido-Reductase from *D. gigas*

Maria J. Romão, Margarida Archer, Isabel Moura, José J. G. Moura, Jean LeGall, Richard Engh, Monika Schneider, Peter Hof, Robert Huber*

The crystal structure of the aldehyde oxido-reductase (Mop) from the sulfate reducing anaerobic Gram-negative bacterium *Desulfovibrio gigas* has been determined at 2.25 Å resolution by multiple isomorphous replacement and refined. The protein, a homodimer of 907 amino acid residues subunits, is a member of the xanthine oxidase family. The protein contains a molybdopterin cofactor (Mo-co) and two different [2Fe-2S] centers. It is folded into four domains of which the first two bind the iron sulfur centers and the last two are involved in Mo-co binding. Mo-co is a molybdenum molybdopterin cytosine dinucleotide. Molybdopterin forms a tricyclic system with the pterin bicycle annealed to a pyran ring. The molybdopterin dinucleotide is deeply buried in the protein. The *cis*-dithiolene group of the pyran ring binds the molybdenum, which is coordinated by three more (oxygen) ligands.

Molybdenum is an essential element for microbial, plant, and animal life. Except in the nitrogenases where it is part of a heterometal molybdenum-iron-sulfur cluster, the metal is usually associated with a pterin derivative to form the molybdenum cofactor (Mo-co) (*1*). Mo-co containing enzymes participate in hydroxylation and oxo-transfer reactions that are two-electron transfer processes occurring at the Mo-co site. Water is the ultimate source of the oxygen atom incorporated into the substrate, and reducing equivalents are generated in this process. These features are characteristic of the molybdenum containing hydroxylases and differ from other dioxygen consuming systems. Mo-co enzymes usually contain other redox-active cofactors, such as iron-sulfur clusters, flavins or heme centers, which mediate electron transfer from Mo-co to the final electron acceptor (*1*, *2*).

The aldehyde oxido-reductase (Mop) from the sulfate reducing anaerobic bacterium *Desulfovibrio gigas* contains Mo-co and two different iron-sulfur centers defined by electron paramagnetic resonance (EPR) and Mössbauer spectroscopies as [2Fe-2S] clusters (*3*). This protein was characterized and crystallized (*4*), and its gene was cloned and sequenced (*5*), revealing its relation to xanthine oxidases.

Mop is a homodimer with 907 amino acid residues per monomer. It oxidizes aldehydes to carboxylic acids, with little specificity for the nature of the side group. Mop is part of an electron transfer chain, consisting of four proteins from *D. gigas*, flavodoxin, cytochrome, and hydrogenase such that the oxidation of aldehydes is linked to the generation of hydrogen (*6*). In xanthine oxidases, which have about 1300 amino acid residues, there is electron transfer from the Mo site to a flavin group, associated with a large protein domain absent in Mop.

Chemical studies of derivatives of molybdopterin isolated from xanthine oxidase and

M. J. Romão and M. Archer are at the Instituto de Tecnologia Química e Biológica, Rua da Quinta Grande, 2780 Oeiras and I. S. T., Departamento Química, 1096 Lisboa Codex, Portugal. I. Moura and J. J. G. Moura are in the Departamento de Química (and CQFB) Faculdade de Ciências e Tecnologia, Universidade Nova de Lisboa, 2825 Monte de Caparica, Portugal. J. LeGall is in the Department of Biochemistry and Molecular Biology, University of Georgia, Athens GA 30602, USA. R. Engh, M. Schneider, P. Hof, and R. Huber are at the Max-Planck-Institut für Biochemie, Am Klopferspitz, D-82152 Martinsried, Germany.

*To whom correspondence should be addressed.

sulfite oxidase have suggested a 6-alkyl pterin with a four-carbon side chain containing an enedithiol (at C7′ and C8′), a hydroxyl group (at C9′), and terminal phosphoryl functions. The molybdopterin is in the dihydro state within the enzyme (*7*). The terminal phosphoryl group is replaced by a dinucleotide in some bacterial molybdoproteins (*8*, *9*).

The crystal structure analysis of a tungstoprotein aldehyde oxidoreductase (*10*) confirmed the metal (tungsten) coordination to the *cis*-dithiolene group, but showed, unexpectedly, a tungsten dimolybdopterin cofactor. The tungstoprotein shares no homology to Mop or xanthine oxidases so that the question of the nature of Mo-co remained open.

The crystal structure analysis of the aldehyde oxido-reductase from *D. gigas* shows the structure of Mo-co in atomic detail and allows a first look at a member of the xanthine oxidase family.

Structure determination. The original Mop crystals in space group $P6_122$ with $a=b=$ 144.5 Å, $c=$ 163.2 Å diffracted to about 3 Å resolution after buffer exchange as described (*4*). Their crystalline order and radiation stability was further improved by slow cooling to about −15°C, just above the freezing point of the buffer solution. The crystal quality was variable, and the resolution obtained differed among the crystals. Isomorphous replacement analysis was hampered by the variability of crystals and by nonisomorphism, which was not reflected in the unit cell dimensions. Derivatives were compared with either data set NATI and MOHO, and the one with the smaller intensity differences was chosen as parent compound. Heavy atom positions were derived from difference Patterson maps cross-phasing, and difference Fourier maps and were refined. Phasing statistics indicated very poor phases, which were not substantially improved by combining NATI and MOHO phase sets. The calculated map vaguely showed the molecular boundary and some secondary structures. An imaginary map revealed both iron clusters as the highest peaks. Model building and refinement by phase combination of isomorphous and partial model phases did not progress until two measures were taken. (i) Crystals had been obtained of the aldehyde oxidoreductases from *D. desulfuricans* (ATTC 27774), a species related to *D. gigas* (Mod crystal). These crystals were analyzed with the use of the Mop model. Although, as became clear later, the model was inadequate in many places, averaging of the Mop density calculated with phases combined from isomorphous replacement and model calculations and the model-phased Mod density resulted in improvement, and more structural elements were recognized. (ii) The density was modified by solvent flattening and histogram matching with the use of CCP4 (*11*). This improved the Mop density which was averaged with Mod.

Although the model building was tedious, it was continued and used for phasing. At some stage the amino acid sequence was recognized for two segments beyond the two iron domains that had been identified earlier. This established a number of connectivities and finally led to the complete model of the protein and the cofactors. Refinement was done with different data sets NATI, MOHO, DIEG, and HG00 to their respective resolutions. Water molecules (437) were incorporated on the basis of difference density and stereochemical considerations (Table 1). There were a few outliers in the Ramachandran plot. All were well defined and, except one, were close to the cofactors. The electron density of a $2F_o - F_c$ map was continuous at the 1σ

Table 1. Collection of data and statistics of structure determination and refinement. Data were collected with a Mar Research imaging plate system installed on a Rigaku rotating anode generator and evaluated with MOSFILM (*36*) and CCP4 (*11*). The crystallographic calculations were performed with PROTEIN (*37*) and the density modifications with CCP4. Model building was done with FRODO (*38*) and refinement with X-PLOR (*39, 40*). The data were usually measured from one crystal. The highest resolution was obtained with HG00 to 2.25 Å, which was used for the final refinement. The MOD protein crystallizes in space group $P6_122$ with cell constants of $a = b = 157.2$ Å, $c = 178.6$ Å. A Patterson search performed with these data with the use of X-PLOR and the available Mop model revealed the orientation. The translation function yielded the translation parameters (*41*). The Mod crystal data have been refined at 3.5 Å resolution starting with the transformed Mop model. No sequence is available for Mod.

Data set*	Reflections		R_s†	Resolution		Binding sites (*N*)‡	Phasing power§	⟨*I*⟩/⟨σ*I*⟩ (last shell)
	Total	Unique		Å	Completeness (%)			
NATI	264226	23936	0.087	2.8	95.2			1.6
MOHO	236858	28733	0.039	2.6	92.0			3.0
DIEG	143765	24967	0.048	2.7	97.0			4.5
PTC1	108146	24057	0.060	2.8	91.3	3	0.61	
YBSO	47976	19366	0.106	2.9	79.9	1	0.38	
IRNC	24679	9740	0.118	3.8	87.9	2	0.47	
PTPT	36321	8188	0.073	3.9	85.0	5	0.78	
PTYB	30342	12840	0.113	3.3	85.0	5	0.47	
UOOX	34082	12169	0.126	3.5	86.3	2	0.52	
MOCN	54013	21547	0.126	2.8	78.7	4	0.25	
HGSC	11991	4655	0.101	4.6	78.1	3	0.88	
OSCL	47462	20672	0.064	2.8	78.5	4	0.48	
IRRE	91444	21082	0.075	2.9	89.0	1	0.27	
HG00	251090	47579	0.090	2.25	92.7	1	0.26	3.8
PCL4	40320	13798	0.093	3.15	76.7	4	1.12	
MOD	31599	16643	0.079	3.5	97.9			

Model	HG00	MOHO	DIEG	MOD crystal
R factor (%)	16.5	15.4	14.2	26.0
Last shell	29.4	24.2	21.6	
Resolution (Å)	10.0–2.25	10.0–2.6	10.0–2.7	10.0–3.5
Free *R* factor‖	23.3			
rms bonds (Å)¶	0.009	0.009	0.009	0.009
rms angles (°)¶	1.9	1.9	1.9	2.8
	Protein	Mo-co	Fe-S	Solvent
Average temperature factor (Å²)	30.9	31.1	30.2	28.5

*The harvesting buffer (hb) was: 0.2 M Hepes, 0.2 M $MgCl_2$, 30 percent PEG 4000, 30 percent isopropanol, pH 7.2; all crystals were in this buffer. NATI, native crystals; MOHO, native crystals co-crystallized with 2 mM $K_4Mo(CN)_8$; DIEG, native crystals co-crystallized with 10 percent diethylene glycol; PTC1, soak 24 hours with K_2PtCl_4 (1 mg/ml); YBSO, soak 2 days in 2.5 mg of $Yb_2(SO4)_3$; IRNC, soak 4 days in 4.0 mg of $Ir(NH_3)_5Cl_3$, 3.0 mg of $IrCl_6K_3$; PTPT, soak 4 days in saturated $Pt(NH_3)_2(NO_2)_2$; PTYB, soak 1 day in 3.6 mg of K_2PtCl_4, 1.4 mg of $Yb_2(SO_4)_3$, 1.9 mg of $Gd_2(SO_4)_3$; UOOX, soak 2 days in 2.1 mg of UO_2NO_3, 3.5 mg of $K_4U(C_2O_4)_4$; MOCN, soak 3 days in $K_4Mo(CN)_8$ (2 mM); HGSC, soak 4 hours in 1.1 mg of $[(CH_3Hg)_3S]_2Cr_2O_7$; OSCL, soak 2 days in K_2OsCl_6 at 1 mg/ml; IRRE, soak 1 day in saturated solutions of $K_3Ir(NO_2)_6$ and K_3ReCl_6; HG00, native crystals cocrystallized with PCMBS at 1 mg/ml; PCL4, soak 15 hours in K_2PtCl_4 at 5 mg/ml. †$R_2 = \Sigma\ (I-\langle I\rangle)/\Sigma I$, where I is the measured intensity and $\langle I\rangle$ is the averaged value; the summation is over all measurements. ‡Heavy atom binding sites. §Phasing power, F_H/residual: rms mean heavy atom contribution/rms residual, defined as $[(F_{PHcalc}^2 - F_{PH}^2)/N]^{1/2}$ with the sum over all reflections, where F_{PHcalc} is the calculated structure factor and F_{PH} is the structure factor amplitude of the heavy atom contribution, respectively. ‖Free *R* factor, calculated by setting aside 5 percent of the reflections in the final stages of refinement after extensive simulated annealing. ¶The rms deviations from ideal values.

level except between residues 723 and 724. This segment was exposed and had high temperature factors.

The polypeptide structure. The molecule is globular and the average diameter is 75 Å (Fig. 1). The secondary structure has 28 percent helical and 21 percent β-sheet conformation as defined by the program DSSP (*12*). There are 33 helical and 27 β-strand segments longer than three amino acid residues. Mop is organized in four domains (Fig. 2) consisting of the NH_2-terminal, the first [2Fe-2S] domain (residues 1 to 76), the second [2Fe-2S] domain (residues 84 to 157), and an extended connecting peptide from residues 158 to 195 which leads into the large Mo-co domain from residues 196 to 907. This domain is subdivided into (i) the Mo1 domain (residues 196 to 581), which contributes with two molybdopterin binding segments and (ii) the Mo2 domain, which provides a third, and all of the dinucleotide binding segments (582 to 907).

The chain fold of the first iron domain resembles that of the plant and cyanobacterial [2Fe-2S] ferredoxins from *Spirulina platensis* and *Anabaena*, respectively (*13*). It is formed by a five-stranded β half-barrel (s1_4, s1_3, s1_5, s1_1, s1_2) enclosing an α helix (h1_1) orthogonal to the strand directions. It has the first β turn between s1_1 and s1_2 shorter by six residues (residues 9 to 14) and lacks the loop 54 to 73, when compared to ferredoxin; but the iron-sulfur cluster binding turns closely match in the two structures.

The second iron domain has a previously undescribed [2Fe-2S] ferredoxin-type fold, a

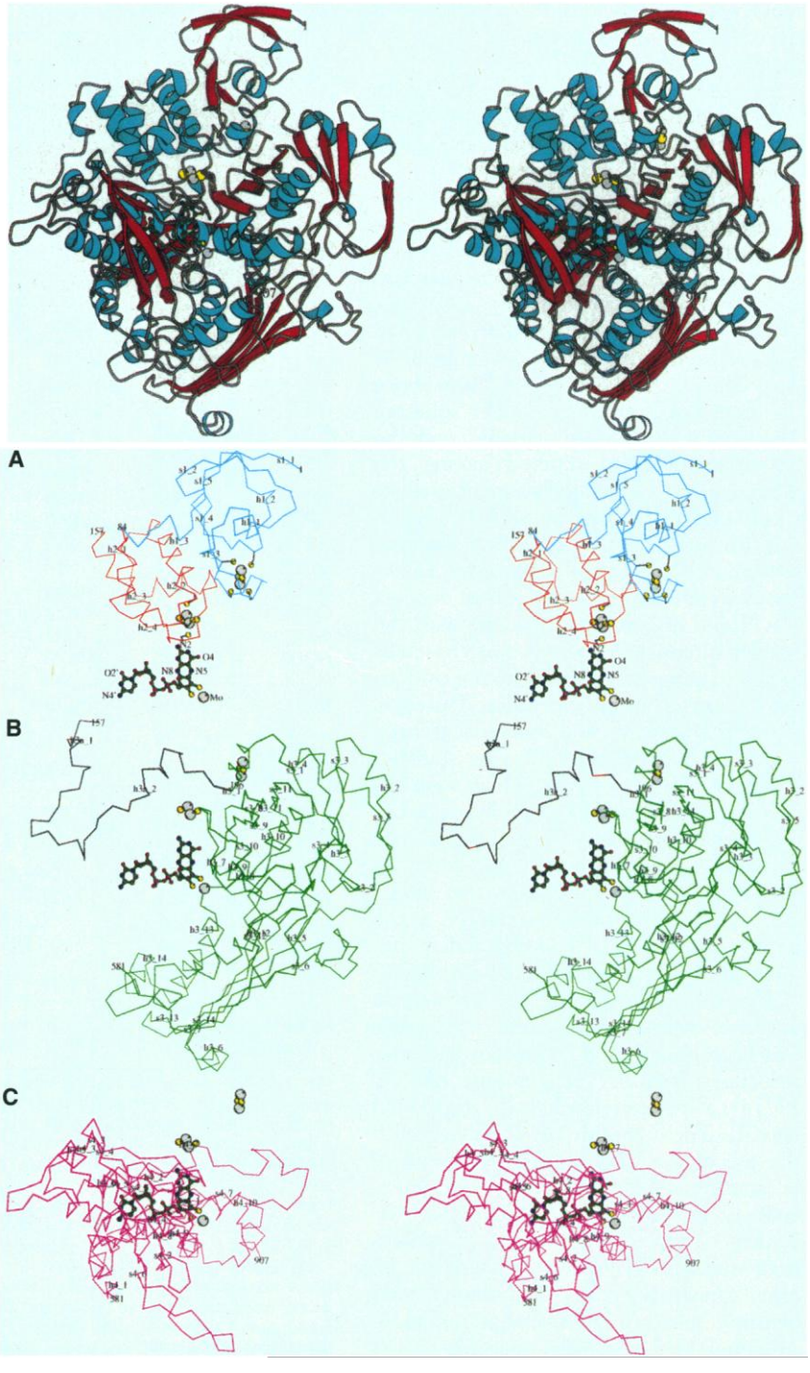

Fig. 1 (**top**). Molecular structure and helical (blue) and β-sheet (red) secondary structures drawn with MOLSCRIPT (*42*). The sulfurs of the cofactors are yellow, and the metal atoms are silver. The substrate binding tunnel is in the middle lower third. The view is onto the molybdenum from an approaching substrate. **Fig. 2** (**bottom**). Secondary structures were calculated with DSSP program (*12*). Listed and labeled are segments with at least three residues. Strands are designated as s and (α or 3_{10}) helices as h. The number indicates the domain in which this segment is located and is followed by a serial number. 1, first [2Fe-2S] domain; 2, second [2Fe-2S] domain; 3, connecting segment and Mo1 domain; 4, Mo2 domain. The assignment of the first and second iron domains to the spectroscopically distinguishable iron-sulfur centers. FeS1 and FeS2 has been unclear. Data of magnetic coupling, electron transfer rates, redox potentials, and accessibility support FeS1 as second and FeS2 as first domain. s1_1, 2–8; s1_2, 11–17; h1_1, 23–29; s1_3, 49–52; s1_4, 55–58; h1_2, 64–66(3_{10}); s1_5, 72–74; h1_3, 76–79; h2_1, 87–94; h2_2, 104–117; h2_3, 123–132; h2_4, 143–156; h3a_1, 162–165(3_{10}); h3a_2, 185–190; h3_1, 196–201; s3_1, 208–214; s3_2, 220–226; h3_2, 228–232; s3_3, 236–241; h3_3, 242–244(3_{10}); s3_4, 281–287; h3_4, 290–298; s3_5, 301–306; h3_5, 313–317; s3_6, 331–339; h3_6, 343–348; s3_7, 352–360; s3_8, 372–377; s3_9, 383–387; h3_7, 392–403; h3_8, 407–409(3_{10}); s3_10, 410–414; h3_9, 423–425(3_{10}); h3_10, 429–440; s3_11, 444–447; h3_11, 450–455; s3_12, 463–471; s3_13, 477–478, h3_12, 495–505; s3_14, 515–522; h3_13, 537–555; h3_14, 559–566; h4_1, 585–606; s4_1, 611–624; s4_2, 631–639; s4_3, 643–647; h4_2, 657–668; h4_3, 676–678(3_{10}); s4_4, 679–681; h4_4, 700–719; h4_5, 729–734, s4_5, 740–746, s4_6, 765–778, s4_7, 783–794; h4_6, 801–820; h4_7, 841–843(3_{10}); s4_8, 848–852; h4_8, 870–872(3_{10}); h4_9, 875–887; h4_10, 898–905. (**A**) Cα trace of the first (blue and second (red) FeS domains including the cofactors. The view for this and for (A) and (B) is the same as in Fig. 1. (**B**) The connecting segment (black) and Mo1 domain (green). (**C**) The Mo2 domain (purple).

twofold symmetric four-helix bundle, with the iron-sulfur cluster located at the NH_2-termini of the longer central helices h2_2 and h2_4.

The connecting peptide spans between the exit of the second iron domain and the entry into the molybdenum domain. It is loosely folded with two short two-turn helical segments h3a_1 and h3a_2 attached to the iron domain.

The Mo1 domain is banana-shaped, 75 Å long and 28 Å thick. The lower, thinner stem part consists of a five-stranded antiparallel parallel β sheet (s3_6, s3_14, s3_13, s3_12, s3_7), which is flanked by two α helices (h3_12, h3_13) running roughly parallel to the strand directions on the one side and exposed to solvent on the opposite side. The thicker upper head part has a seven-stranded parallel, antiparallel incomplete β barrel with strands s3_3, s3_4, s3_1, s3_11, s3_8, s3_9, s3_10, whose central cavity is occupied by an α helix, h3_10. It is partly covered by the exposed helices h3_2 and h3_4. Two segments span the Mo1 domain along its entire length.

The Mo2 domain is organized in two wings spanning 82 Å. The cofactor lies at the intersection of the wings. These form αβ structures and have two strands traversing the entire domain. The dominant construction element of the wings, which have a similar basic fold and are in part diad related, are four-stranded β sheets with strands s4_5, s4_2, s4_3, s4_4 (the front wing) and strands s4_1, s4_6, s4_7, s4_8 (the back wing). The sheets bend around two helices in each wing, h4_2 and h4_4 (front wing) and h4_6 and h4_8 (back wing), respectively.

The first and the second iron domains cohere by interaction of helix h2_2 of the latter with the β sheet of the former. They have little noncovalent contact to the Mo1 domain, but the Mo2 domain has a substantial area of contact with both and may clamp.

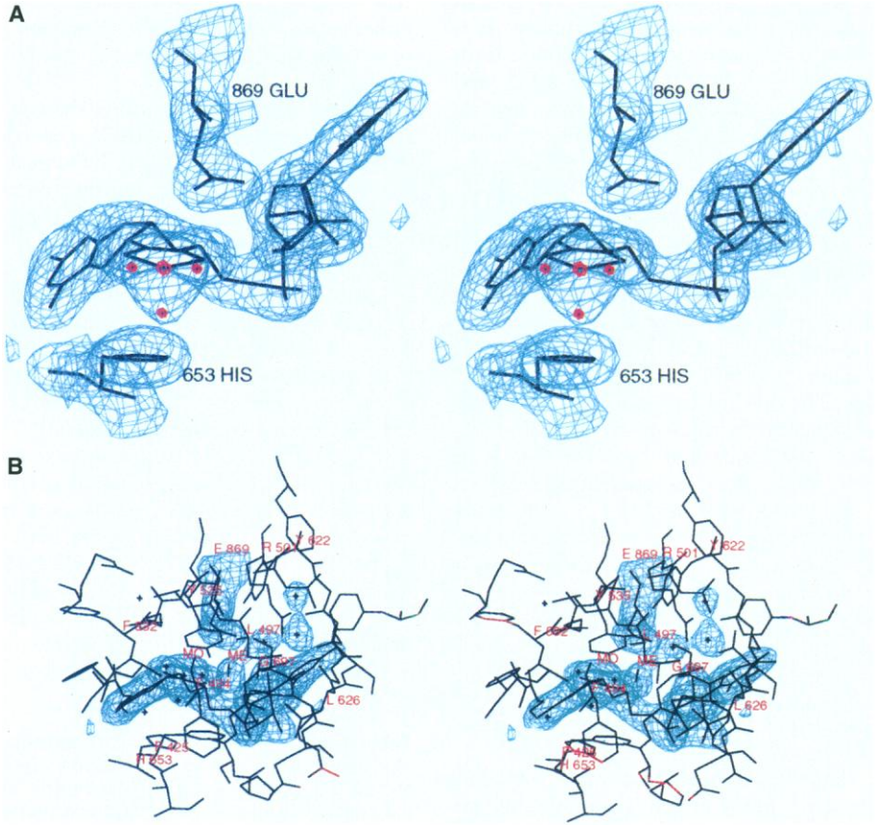

Fig. 3. (**A**) Electron density at 1σ of the $2F_o - F_c$ map around the Mo-co and Glu^{869} and His^{653}. The molybdenum and its three oxygen ligands are drawn as red balls. (**B**) Electron density around Mo-co, Glu^{869}, and the water chain and surrounding model as seen from the substrate tunnel. The side pocket with the three water molecules extends toward the upper right corner. The disk-shaped density is marked ME.

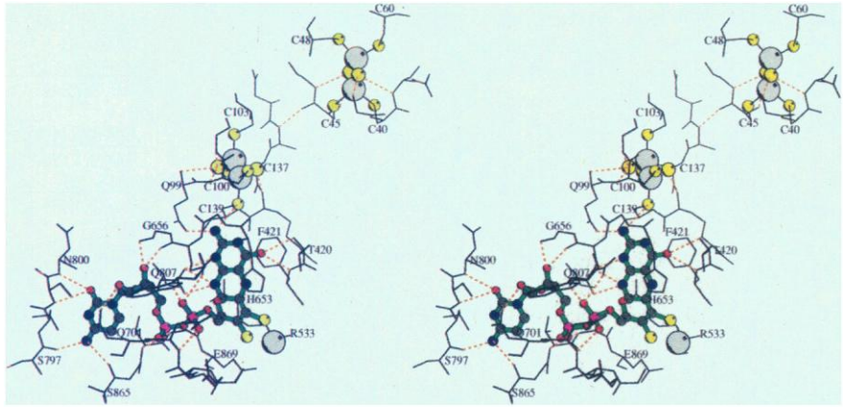

Fig. 4. Stereo drawing of the molybdopterin cytosine dinucleotide, the second [2Fe-2S] (**middle**), and first [2Fe-2S] cluster (**top**), and their contacting residues in the orientation of Fig. 1. Hydrogen bonds are indicated by broken red lines.

Structure and binding of the cofactors. The electron density for all cofactors is well-defined. Mo-co in Mop is a molybdenum molybdopterin cytosine dinucleotide as shown in the electron density (Fig. 3) and confirmed by chemical analysis (*14*). It is in an extended conformation, at variance with the suggestion by Chan *et al.* (*10*) of an involvement of the sugar hydroxyl groups in molybdenum binding. The functional groups of the cytidine are hydrogen bonded to main chain atoms (Fig. 4). The cytosine dinucleotide has the pyrimidine base in *anti* conformation and the D-ribofuranose twisted with C2″ endo and C3″ exo.

The molybdopterin has two fused ring systems, namely, the bicyclic pterin and the monocyclic pyran system as had also been observed in tungsten dimolybdopterin (*10*). In that isolated molybdopterin derivatives have an open side chain at C6, ring closure may occur in situ where a tricycle is stabilized by numerous interactions with the protein. Ring formation is facile for the 5,8-dihydromolybdopterin by nucleophilic addition of O9′ to C7 of an imine tautomer. An open chain cofactor has fewer steric restrictions and might facilitate protein cofactor assembly. The formation of urothione, a metabolite of molybdopterin excreted in urine might follow a similar route by addition of the S8′ atom of a (*trans*) dithiolene group to C7 generating a thiophen ring.

In the tricycle, the pterin and pyran rings enclose an angle of about 40°. The pyrazine part of the pterin ring system is

twisted, with C6 exo and C7 endo. The pyran ring has envelope conformation with O9′ endo. Its three chiral centers at C6, C7, and C9′ have been modeled as R, R, R. Tight packing in the protein interior of the twisted tricyclic Mo-co is incompatible with binding (and formation) of a fully oxidized species with a planar pterin ring system. The tricycle, in contrast, is formally a tetrahydro species. The pterin system is so rendered redox inactive as is observed (*15*).

The *cis*-dithiolene group and the molybdenum form the equatorial plane of the metal ligands. Mo (VI), present in the oxidized form of the enzyme, is penta-coordinated by two (dithiolene) sulfur and three oxygen ligands (Fig. 3A). There is a disk-shaped electron density close to the equatorial ligand trans to S7′ representing an unidentified molecule from the crystallization solution. It is also close to a chain of three water molecules located in a side pocket (Fig. 3B). The oxygen ligand trans to S7′ is hydrogen-bonded to the amide group of G697 (3.0 Å). The fourth equatorial oxygen ligand trans to S8′ has the amide nitrogen of R533 (3.3 Å), the carbonyl oxygen of F421 (3.8 Å), and the Cα of G422 as closest neighbors. An axial ligand is in the vicinity of H653 and in long hydrogen bond distance to the carbonyl oxygen of S695 (3.6 Å). On the opposite side, the Glu axial ligand site is vacant. The carboxylate group of E869 is not a ligand to the metal (3.5 Å) but could, by a slight rotation, bind to it. We suggest that E869 is protonated.

The molybdenum center of xanthine oxidase contains a cyano-lysable sulfur, which is essential for catalysis. The desulfo enzyme is inactive (*16*).

The EPR and EXAFS (extended x-ray absorption fine structure) spectra of Mop indicated close similarity to the desulfo form of xanthine oxidase, but the functional enzyme is believed to be a sulfo form also (*6*, *17*, *18*). There is no sulfur ligand in the electron density of Mop and Mop and xanthine oxidase have no cysteine residue close to the molybdenum (Table 2). EXAFS data for xanthine oxidase have been interpreted as a monoxo, monohydrosulfido, or monohydroxo (for the desulfo form) structure in the Mo(IV) state and a monoxo, monothio, or a dioxo (in the desulfo enzyme) structure in the Mo(VI) state (*19*, *20*). We expect a dioxo structure for (desulfo) Mop in the oxidized state. Of the three available sites, the axial His and the trans S7′ equatorial positions are much less spatially constricted than the site trans to S8′. One of them may be the cyanolysable sulfur site because it could harbor a larger and more distantly bonded sulfur atom.

Fe1 of the second iron cluster is linked to C100 and C139, Fe2 to C103 and C137. The plane of the [2Fe-2S] group is orthogonal to the plane of the cysteine sulfurs. The irons are thus tetrahedrally coordinated by sulfur atoms. The first iron cluster has Fe1 and Fe2 linked to C40 and C45 and C48 and C60, respectively, and is similar to the second. The iron-sulfur bond lengths are 2.2 Å from the irons to the sulfides and 2.3 Å to the cysteine Sγ.

The second [2Fe-2S] center is buried about 15 Å beneath the nearest protein surface and has no access to solvent. It is sequestered between two polypeptide turns connecting helices h2_1 and h2_2 and h2_3 and h2_4, respectively, whose peptide amide groups point toward the cluster under formation N-H. . . . S hydrogen bonds. The first [2Fe-2S] center is close to the protein surface and its Sγ 60 is exposed to solvent. It is located between two turns preceding s1_3 and linking s1_4 and h1_2, respectively. Its sulfurs are hydrogen bonded to main chain amide groups (Fig. 4). The dinucleotide of Mo-co is solely bound by the Mo2 domain. It is buried 7 Å beneath the surface. The cytidine base is specifically recognized mainly by the loop between s4_7 and h4_6 and forms four hydrogen bonds to main chain atoms mentioned above. The loop linking s4_8 with h4_8 contributes one more hydrogen bond. The ribose hydroxyl groups are hydrogen-bonded to main chain and side chain oxygens. The pyrophosphate moiety is sequestered and hydrogen-bonded to the amino ends of two helical segments h4_4 and h4_8 and to N^{ε} atoms of W650 and Q655. There is no positively charged residue in direct contact with it.

The tricyclic molybdopterin is buried in the center of the protein accessible through a 15 Å deep tunnel. It interacts with its N5 edge with the Mo1 domain and with its N8 side with the Mo2 domain by hydrogen bonds of which N2 to Sγ of C139, an iron ligand of the second cluster is particularly significant. The F421 phenylalanine ring is coplanar to the pterin with appropriate distances (3.4 Å) for π-π interactions. The tunnel leading from the protein surface to the molybdenum is funnel-shaped, wide at the upper rim and narrowing toward the metal site. The right-hand side of the tunnel wall includes residues of the Mo1 domain, while residues of Mo2 form the left-hand side. The coating of the tunnel walls is apolar with: L254-, I255-, I390-, L394-, Y397-, G422 or G804, F425 or E807, F494-, L497-, R501-, A531 or A915, Y535 or F919, Y622 or Y1010, L626 or F1014, D627 or G1015, N691 or N1078, P694 or P1081, G696 or A1083, G697 or A1084, H752- [homologous residues in xanthine oxidase are given (as or) when a reliable alignment is possible]. The tunnel has a narrow constriction at half height by residues F425, F494, L497, L626, which must swing away to let larger (aromatic) aldehydes pass (Fig. 5). The molecular structure, if unperturbed, seems to allow passage only of small aliphatic aldehyde substrates, which Mop prefers (*6*), but the side chains of Y622 and R501 might give away to accommodate larger ligands. The tunnel constriction would also not seem to allow passage of the molybdopterin cytosine dinucleotide cofactor. Protein cofactor association therefore requires either substantial structural rearrangements or sequential domain folding, cofactor binding, and domain assembly.

Xanthine oxidase. Xanthine oxidase of *Drosophila melanogaster* (DMXO) is encoded in the *rosy* locus and has been the subject of intensive studies concerning gene structure and regulation and electrophoretic variants of the expressed proteins (*21*). The similarity or identity in amino acid sequence between Mop and xanthine oxidase is 52 percent or 26 percent (*5*, *21*), indicating a close structural relationship. The sequence similarity is particularly high in those segments associated with the iron-sulfur centers and the molybdopterin (Table 2). The contacts between the cytosine dinucleotide portion and the protein are less conserved with some conspicuous replacements between the two proteins: G660/K1050, T803/D1197, C798/L1191, A802/I1196. These residues point toward ribose and base and, being bulkier in xanthine oxidase, might fill the cavity when the dinucleotide is absent. It is surprising that members of

Table 2. Comparison of contacting segments in Mop and Xanthine oxidase as indicated from EPR and EXAFS. The cofactor FeS_B is the first, and the cofactor FeS_A is the second iron domain. Abbreviations for the amino acid residues are: A, Ala; C, Cys; D, Asp; E, Glu; F, Phe; G, Gly; H, His; I, Ile; K, Lys; L, Leu; M, Met; N, Asn; P, Pro; Q, Gln; R, Arg; S, Ser; T, Thr; V, Val; W, Trp; and Y, Tyr.

Contacting segments	MOP and DMXO
FeS_B	
CEQGQCGAC	MOP (40–48)
CAEGGCGAC	DMXO(43–51)
ACVT	MOP(59–62)
ACLT	DMXO(72–75)
FeS_A	
QCGFCSPG	MOP(99–106)
QCGFCTPG	DMXO(112–119)
NACRCTGYKP	MOP(135–144)
NLCRCTGYRP	DMXO(146–155)
Molybdopterin	
GGTFGYK	MOP(418–424)
GGGFGGK	DMXO(800–806)
AFRGYGAPQSM	MOP(531–541)
AFRGFGGPQGM	DMXO(915–925)
HGQG	MOP(653–656)
IGQG	DMXO(1043–1046)
GPSGGS	MOP(693–698)
SPTAAS	DMXO(1080–1085)
VGELPL	MOP(867–872)
VGEPPL	DMXO(1265–1270)

the same protein family may bind molybdopterin monophosphates and cytosine dinucleotides as eukaryotic xanthine oxidases and Mop do.

Mop lacks the FAD (flavine adenine dinucleotide) domain present in xanthine oxidase. The comparison of amino acid sequences had suggested an insertion of 387 residues between residues 176 and 177 of Mop. Thus the FAD domain may replace the connecting segment in Mop and be located in the shallow dish-like depression between the iron, Mo1, and Mo2 domains in contact with all three (Fig. 2). The NAD binding site in chicken liver xanthine dehydrogenase has been chemically labeled with a reactive analog at Y395 (DMXO numbering) (*22*), which lies within this insertion.

The substrate binding pocket at the molybdenum site seems well conserved between Mop and xanthine oxidase except a replacement of F425 or E807; this is well positioned to bind to imino functions of xanthine and related substrates and may be the determinant for the substrate specificity of xanthine oxidase for which many different classes of inhibitors have been synthesized and studied for therapeutic use (*23*).

Other proteins, such as sulfite oxidase and nitrate reductase contain Mo-co. Their sequences are closely related but show only weak homology to xanthine oxidase (*24*). They lack the signature sequences shown in Table 2 and probably display a different mode of cofactor binding.

Enzyme mechanism. The molybdopterin containing enzymes catalyze two-electron redox reactions whereby a net exchange of an oxygen atom between substrate and water occurs. Two electrons and two protons are released in this process and the molybdenum cycles through oxidation states VI, V, and IV, such that $RH + H_2O \rightarrow ROH + 2\ H^+ + 2e^-$ (*25*). By single turnover experiments in xanthine oxidase it was shown that transfer of a firmly bound oxygen to substrate takes place within the reductive half-cycle of the reaction whereby Mo(VI) becomes Mo(IV) (*2*, *26*). Synthetic model systems are available for such a process (*27*). In the oxidative half-cycle of the reaction Mo(VI) is regenerated by two one-electron processes and the transferred oxygen replaced by water. The presence of bound substrate or product in the Mo(VI) and Mo(IV) center of xanthine oxidase is suggested by EXAFS (*19*, *20*) and in the Mo(IV) center also by resonance Raman studies (*28*).

On the basis of the structural features described and on model considerations, we suggest a reaction mechanism for Mop whereby the aldehyde substrate binds to the molybdenum with its carbonyl oxygen close to the vacant axial Glu site and to (the protonated) Glu^{869}. This may facilitate addition of oxygen at the carbonyl carbon atom associated with transfer of reducing equivalents generating the carboxylic acid which may be transiently bound as a bidentate ligand. Such binding was suggested for the aldehyde inhibited structure of xanthine oxidase (*29*). Simple modeling with benzaldehyde/benzoic acid, given the severe steric restrictions at the molybdenum (Figs. 3B and 5), agrees with such binding at a site that overlaps partially with the disk-like density mentioned earlier. The transferred oxygen may be one of the molybdenum ligands or the nearest molecule of the chain of waters. Release of the carboxylic acid product follows, perhaps facilitated by Glu^{869} binding to the metal. The ensuing oxidative half-reaction involves one-electron transfers from the molybdenum to the iron centers. Protons are released in this process whereby Glu^{869} and the product carboxylic acid may act as bases.

Similar modeling was carried out with xanthine assuming that initial binding occurs with N7 near to the Glu axial site. The reaction could then proceed as with the aldehyde, and the oxygen added to C8. Such binding would be consistent with EXAFS data of 8-bromoxanthine bound to xanthine oxidase that place the bromine 4 Å away from the molybdenum (*30*). The mechanism proposed has features in common with a suggestion by Bray (*31*). We assign a central role as hydrogen bond donor and as transient metal ligand to Glu^{869}, which is totally conserved in the xanthine oxidase family (Table 2).

The electrons are transferred from the molybdenum center to the FAD cofactor in xanthine oxidase, which is oxidized by NAD^+ in the dehydrogenase form or by dioxygen in the oxidase form (*1*) and to some unknown acceptor in Mop which lacks the FAD domain. The molecular structure delineates the electron transfer pathway from the molybdenum to the iron-sulfur centers. Electron exchange may occur through the partially conjugated system of the molybdopterin and the N2–Sγ139 hydrogen bond to the second iron center via covalent and hydrogen bonds along the pathway Fe1–C45–O. . . . . HN-A136 - C137 - Fe2 (first iron center) (Fig. 4). In that the redox centers are close and connected by bonds, electron transfer is governed by energetics (redox potentials) and reorganization energy. We know little of the latter, but the [2Fe-2S] structure of the iron-sulfur centers is probably inert toward valence changes similar to plant ferredoxins. The molybdenum center may have more freedom to move and the mechanism outlined might require modification because of effects of bond formation, bond order changes, and proton transfers. The measured oxidation-reduction potentials (*32*) indicate a substantial driving force in xanthine oxidase and Mop (*6*). Experimental data of electron transfer rates in xanthine oxidase by pulse radiolysis (*33*) and laser flash photolysis (*33*, *34*) seem to agree that internal electron transfer is rapid relative to enzyme turnover and that there is particularly fast electron transfer between molybdenum and FeS1 with a first-order

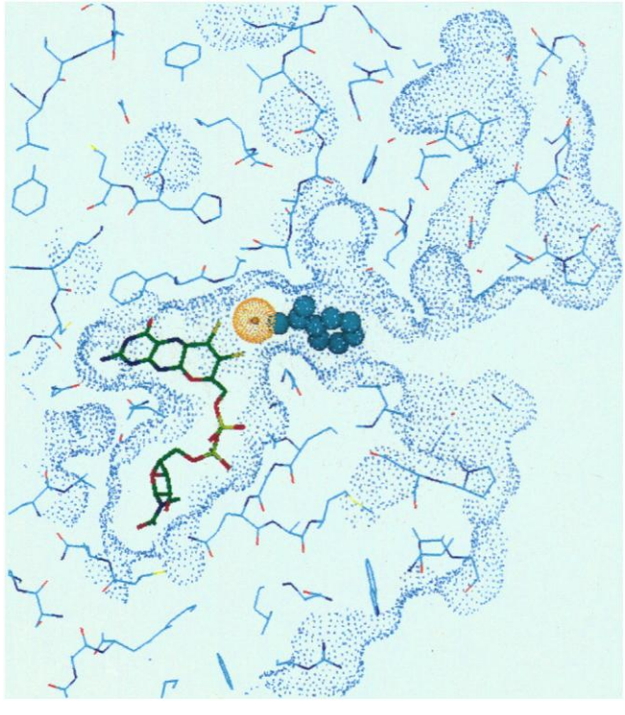

Fig. 5. Molecular surface in van der Waals distance from the atom positions [program MAIN (*43*)]. Slice through the molecule at the Mo-co site with a modeled benzoic acid product bound. The deep and very narrow substrate tunnel opens toward right.

rate constant of $8.5 \times 10^3\ s^{-1}$ (35).

Mop, like all members of the xanthine oxidase family, is a homodimer. The subunits are functionally independent. A comparison of Mop and Mod crystal packings reveals one common diad that generates two symmetrical contacts of mainly hydrophobic character involving M1, I11, F16 and M203, P204, F374, Y376, L199, M203, P443. The cofactors are quite far apart, the closest being the first iron centers with 38 Å.

REFERENCES AND NOTES

1. E. I. Stiefel, *Annu. Chem. Soc. Symp.* **535**, 1 (1993).
2. R. Hille, *ibid.*, p. 22.
3. B. A. S. Barata *et al.*, *Eur. J. Biochem.* **204**, 773 (1992).
4. M. J. Romão *et al.*, *ibid.* **215**, 729 (1993).
5. U. Thoenes *et al.*, *ibid.* **220**, 901 (1994). By the crystallographic analysis, errors were detected in the sequence at two sites. These errors caused reading frame shifts. The sequences suggested from crystallography were then confirmed by nucleotide sequencing. They read: S624/G625LDGPDASEAWAELNADGTITVHTAWEDHGQGADIGCVGTAHEALRPMGVAPEKIKFTWPNTATTPNSGPSGGSR699/Q700 and: G782/Q783TTVDGM789/T790. Mop has 907 residues, one residue more than given by Thoenes *et al*. The sequence numbers have 1 added from Q700 on. We thank O. L. Flores, A. Neves, C. Rodrigues-Pousada, A. Cassing for information about the corrected sequence. The accession number is X77222.
6. B. A. S. Barata, J. LeGall, J. J. G. Moura, *Biochemistry* **32**, 11559 (1993).
7. K. V. Rajagopalan, *Adv. Enzymol. Rel. Areas, Mol. Biol.* **64**, 215 (1991).
8. J. L. Johnson, K. V. Rajagopalan, O. Meyer, *Arch. Biochem. Biophys.* **283**, 542 (1990).
9. O. Meyer, K. Frunzke, J. Tachil, M. Volk, *Amer. Chem. Soc. Symp.* **535**, 50 (1993); K. V. Rajagopalan *Am. Chem. Soc. Symp.* **535**, 38 (1993).
10. M. K. Chan, S. Mukund, A. Kletzin, M. W. W. Adams, D. C. Rees, *Science* **267**, 1463 (1995).
11. Collaborative Computational Project No. 4 (1994); R. Haber *et al. Acta Crystallogr.* **D50**, 760 (1994).
12. W. Kabsch and C. Sander, *Biopolymers* **22**, 2577 (1983).
13. K. Fukuyama *et al.*, *Nature* **286**, 522 (1980); W. R. Rypniewski *et al. Biochemistry* **30**, 4126 (1991).
14. J. Caldeira, I. Moura, M. J. Romao, R. Huber, J. LeGall, J. J. G. Moura, *J. Inorg. Biochem.* **59**, 739 (1995).
15. R. Hille and V. Massey, *J. Biol. Chem.* **257**, 8898 (1982).
16. S. Gutteridge, S. J. Tanner, R. C. Bray, *Biochem. J.* **175**, 887 (1978); V. Massey and D. Edmondson, *J. Biol. Chem.* **245**, 6595 (1970).
17. J. J. G. Moura *et al.*, *Biochem. J.* **173**, 419 (1978); S. P. Cramer, J. J. G. Moura, A. V. Xavier, J. LeGall, *J. Inorg. Biochem.* **20**, 275 (1984).
18. N. Turner *et al.*, *Biochem. J.* **243**, 755 (1987).
19. S. P. Cramer, R. Wahl, K. V. Rajagopalan, *J. Am. Chem. Soc.* **103**, 7721 (1981); S. P. Cramer and R. Hille, *J. Am. Chem. Soc.* **107**, 8164 (1985).
20. N. A. Turner, R. C. Bray, G. P. Diakun, *Biochem. J.* **260**, 563 (1989).
21. T. P. Keith *et al.*, *Genetics* **116**, 67 (1987).
22. T. Nishino and T. Nishino, *J. Biol. Chem.* **264**, 5468 (1989).
23. D. E. Duggan, R. M. Noll, J. E. Baer, F. C. Novello, J. J. Baldwin, *J. Med. Chem.* **18**, 900 (1975).
24. J. C. Wooton *et al.*, *Biochim. Biophys. Acta* **1057**, 157 (1991).
25. R. C. Greenwood, G. L. Wilson, J. R. Pilbrow, A. G. Wedd, *J. Am. Chem. Soc.* **115**, 5385 (1993).
26. R. Hille and H. Sprecher, *J. Biol. Chem.* **262**, 10914 (1987).
27. X. Zhiguong, C. G. Young, J. H. Enemark, A. G. Wedd, *J. Am. Chem. Soc.* **114**, 9194 (1992).
28. W. A. Oertling and R. J. Hille, *J. Biol. Chem.* **265**, 17446 (1990).
29. R. C. Bray and S. Gutteridge, *Biochemistry* **21**, 5992 (1982).
30. R. Hille and R. C. Stewart, *J. Biol. Chem.* **259**, 1570 (1994).
31. R. C. Bray, in *Biological Magnetic Resonance*, J. Reuben and L. J. Berliner, Eds. (Plenum, New York, 1980), vol. 2, pp. 45–84; R. Hille and V. Massey, in *Molybdenum Enzymes*, T. G. Spiro, Ed. (Wiley, New York, 1985), pp. 443–518.
32. J. T. Spence, M. J. Barber, L. M. Siegel, *Biochemistry* **21**, 1656 (1982); J. Hunt, V. Massey, W. R. Dunham, R. H. Sands, *J. Biol. Chem.* **268**, 18685 (1993). The midpoint redox potentials of xanthine oxidase are Mo^{VI}/Mo^{V}, −375 mV; Mo^{V}/Mo^{IV}, −405 mV; FeS_1, −320 mV; FeS_2: −230 mV. In Mop they are: Mo^{VI}/Mo^{V} −450 mV; Mo^{V}/Mo^{IV} −530 mV; FeS_1 −280 mV; FeS_2−285 mV (*6*).
33. K. Kobayashi, M. Miki, K. Okamoto, T. Nishino, *J. Biol. Chem.* **268**, 24642 (1993).
34. M. C. Walker, J. T. Hazzard, G. Tollin, D. E. Edmondson, *Biochemistry* **30**, 5912 (1991).
35. R. Hille and R. F. Anderson, *J. Biol. Chem.* **266**, 5608 (1991).
36. A. G. W. Leslie, MOSFLM Program Abstract of the Crystallographic Computing School, Bischenberg (1990).
37. W. Steigemann, PROTEIN (version 3.1), thesis (Technische Universität, München, Germany, 1974).
38. T. A. Jones, *J. Appl. Crystallogr.* **15**, 23 (1978).
39. A. T. Brünger. X-PLOR (version 2.1, manual, (Yale Univ. Press, New Haven, CT, 1990).
40. R. Engh and R. Huber, *Acta Crystallogr. sect. A*, **47**, 392 (1991).
41. The operation transforming orthogonal coordinates in angstroms (*F*) of Mop into Mod is: matrix, 0.85083 0.297415 −0.433219/ −0.519678 −0.598446 0.609752/ −0.077909 0.743913 0.663720; translation vector, 27.405 Å, 107.869 Å, and 18.847 Å.
42. P. J. Kraulis, *J. Appl. Crystallogr.* **24**, 946 (1991).
43. D. Turk, thesis (Technische Universität, München, Germany, 1992).

44. Supported by JNICT-BMFT project (M.A., M.J.R. and R.H.), by a PRAXIS/BD/2795/94 doctoral grant (M.A.), and by the AvHumboldt Foundation (M.J.R.). We thank P. Matias (for computational assistance), M. A. Carrondo (for laboratory facilities), A. Xavier for discussions with the ITQB team, A. van de Locht and H. Brandstetter for technical advice, S. Liemann, R. Bray (University of Sussex, UK), and J. H. Enemark (University of Arizona, USA) for discussions, the staff of the UGA Fermentation Plant for growing the cells, and B. Barata (ITQB) and R. Duarte (UNL) for help with protein purification. The coordinates have been deposited in the Protein Data Base (Brookhaven) and have tracking number T7184.

24 April 1994; accepted 18 October 1995